Mapping of parent transition-state wave functions into product rotations: An experimental and theoretical investigation of the photodissociation of FNO

Amy Ogai, James Brandon, and Hanna Reisler
Department of Chemistry, University of Southern California, Los Angeles, California 90089-0482

Hans Ulrich Suter and J. Robert Huber
Physikalisch-Chemisches Institut der Universität Zürich, Winterthurerstrasse 190, CH-8057 Zürich, Switzerland

Michael von Dirke and Reinhard Schinke
Max-Planck-Institut für Strömungsforschung, D-3400 Göttingen, Germany

We study experimentally and theoretically reflection-type structures in the rotational distributions of NO following the photodissociation of FNO via excitation of the S_1 state. Exciting quasibound states with zero quanta of bending vibration in the $FNO(S_1)$ state yields Gaussian-type rotational distributions, while excitation of states with one bending quantum leads to bimodal distributions. In the latter case, the ratio of the two intensity maxima depends on the number of NO stretching quanta in the S_1 state. The accompanying calculations employing a three-dimensional *ab initio* potential energy surface for the S_1 state of FNO are performed in the time-dependent wave packet approach. They reproduce the main features of the experimental distributions, especially the bimodality. The analysis of two-dimensional calculations for a frozen NO bond distance shows that the final rotational state distributions can be explained as the result of a dynamical mapping of the stationary wave function on the transition line onto the fragment rotational quantum number axis. Here the transition line is defined as the line which separates the inner part of the $FNO(S_1)$ potential energy surface from the strongly repulsive F + NO product channel.

I. INTRODUCTION

The final state distributions of fragments in collision-free photodissociation contain a wealth of information on the bond breaking mechanism as well as the interfragment dynamics in the exit channel where the fragments irreversibly separate. Deep insight and rigorous comparisons of theory with experiment can be achieved in experiments where the parent molecule is prepared in a well defined quantum state.[1-3] Such experiments can now be performed, either by infrared or visible excitation of the molecule in the ground electronic state before a second photon promotes it into an upper state,[4,5] or by exciting selectively a quasibound (resonance) state in the excited electronic state that subsequently decays via energy redistribution within the transient complex.[2,6] The latter scheme is only applicable, however, if the excited complex lives for at least several internal periods as manifested in a structured absorption spectrum. By changing the initial state one can conveniently investigate the influence of internal excitation within the excited state on the state populations in the fragments.

Rotational excitation of the diatomic fragments in the photodissociation of polyatomic molecules can arise from three sources: overall rotation of the parent molecule, bending vibration within the parent molecule, and, last but not least, the torque imparted by the recoiling partner to the fragment molecule (the so-called *final state interaction*).[7,8] Overall rotation leads merely to a broadening of the final

rotational state distributions and in many cases, especially if the final state interaction is strong, does not reveal much insight into the intra- and intermolecular dynamics. More interesting are the other two sources. In particular, we are interested in how the motion in the bending degree of freedom in the excited state develops into rotation of the product as the bond ruptures, and in how the final rotational state distribution reflects the initial level of bending excitation as well as the overall strength of the rotational coupling.

If the dissociation in the upper state is direct (the lifetime is less than an internal vibrational period) the final rotational state distribution reflects essentially the quantum mechanical distribution of the bending angle in the *ground* electronic state of the parent molecule (*rotational reflection principle*).[3,7-10] The reflection is mediated by the so-called *rotational excitation function*, which in turn mirrors—in a dynamical sense—the strength of the torque imparted to the rotor as the fragments recoil. Since in almost all experiments the parent molecule is in its lowest bending state, it is of no surprise that the final rotational state distribution $P(j)$ has a Gaussian-type shape. There are many experimental examples which substantiate this picture (see Ref. 3, Chaps. 6 and 10), and a particularly relevant system for the present study is the dissociation of ClNO via the S_1 state.[11-13] Similarly, it is plausible that dissociation of excited bending states will lead to multimodal distributions which reflect the nodal structures of the associated bending wave function. The only experimental verification of this prediction is the dissocia-

tion of water in the first continuum, a system for which the exit-channel coupling is rather weak.[14]

If the dissociation in the upper state is indirect (i.e., the lifetime is of several vibrational periods), the reflection principle is still applicable, but in a modified form.[15,16] Provided the fragmentation proceeds through a transition state consisting of a relatively narrow bottleneck, one can assume the final step of the decomposition to start at this transition state. The rotational distribution of the fragment is then a reflection of the continuum wave function on top of the transition state. Since the number of quanta in the bending coordinate within the excited complex determines the angular shape of the transition-state wave function one expects, as in the direct case, the nodal structure to be reflected by the final state distribution of the product.

In most experiments of indirect dissociation, only the lowest bending state within the upper electronic manifold is excited, and therefore $P(j)$ has a Gaussian-type shape as in direct dissociation. Pertinent examples are the photodissociations of CH_3ONO (Refs. 17 and 18) and HONO (Ref. 19) through excitation in their S_1 states. On the other hand, excitation of higher bending states will lead to structured distributions which ultimately reflect the nodal structures of the dissociative wave function as it evolves through the transition-state region. This has been demonstrated in the dissociation of $ClNO(T_1)$.[6,20,21] Excitation of the first two excited bending states of $ClNO(T_1)$ yields bi- and trimodal rotational distributions of the NO fragment, while excitation of the lowest bending state gives rise to a monotonically decreasing distribution that maps the shape of the wave function. These results, which have recently been reproduced by *ab initio* calculations,[22] clearly demonstrate the dependence of the final rotational state distributions on the initial quantum state within the complex.

For $ClNO(T_1)$ the coupling between the rotational and the dissociation coordinate is apparently weak (i.e., only a small torque is imparted by the recoiling partner), with the result that the maxima in the final distributions occur at low rotational states. In this article, we present a combined experimental and theoretical study which shows that reflection-type structures exist even when the exit channel couplings are rather strong. In the photodissociation of FNO through the S_1 state, the maxima in the rotational distributions lie between $j \approx 30$–40.

Figure 1 depicts the measured absorption spectrum. It consists of a main progression which is assigned to excitation of the NO stretching mode (v_1) with quantum numbers $v_1 = 0,1,\cdots$ and a second, less intense progression built on $v_3 = 1$ with v_3 being the bending mode. A more detailed discussion of this spectrum follows in Sec. II. Exciting $FNO(S_1)$ to levels with $v_3 = 0$ consistently yields Gaussian-type rotational state distributions, while corresponding excitations in the $v_3 = 1$ bands produce distinctly bimodal distributions.

Recently Suter *et al.*[23] calculated a two-dimensional potential energy surface (PES) for $FNO(S_1)$ including the two stretching coordinates, and analyzed the spectrum in a time-dependent wave packet study. In the present article we extend these calculations by incorporating also the FNO
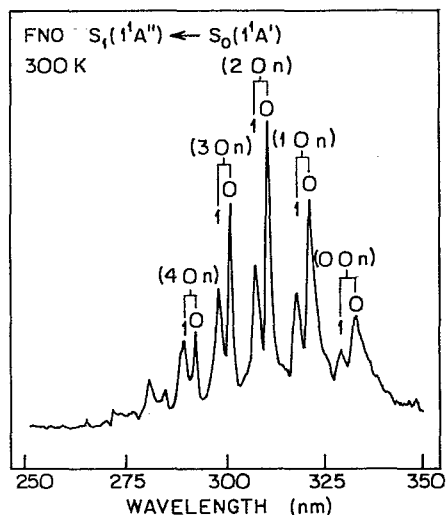

FIG. 1. Measured absorption spectrum of the $S_1 \leftarrow S_0$ transition in FNO recorded at 300 K. v_1 and v_3 are the NO stretching mode and the bending mode, respectively. In the figure $v_3 = n$.

bending angle in order to treat the rotational excitation of the NO fragment and to compare the experimental with the calculated distributions.

The present article is organized as follows. Section II summarizes the experimental details and the results. The potential energy surface, the three-dimensional wave packet calculations, and the resulting rotational state distributions are described in Sec. III. In Sec. IV we elucidate the reflection effect by means of two-dimensional calculations for which the NO stretching degree of freedom is frozen and finally, Sec. V summarizes the findings and conclusions.

II. EXPERIMENTAL RESULTS

A. Experimental details

The experimental arrangement is very similar to the one used previously,[20,24] and only details specific to the present experiment are described. The fluorescence chamber is of octagonal shape, and can accommodate several laser excitation-detection geometries. Premixed FNO samples (FNO:He = 5:1000 Torr) were prepared and expanded in a Ni pulsed valve driven by a piezoelectric crystal (Physik Instrumente, 0.5 mm diam. orifice, ~ 200 μs pulse duration)[25] into the fluorescence chamber, where the FNO was dissociated 15 mm downstream from the nozzle orifice. A Nd:YAG laser-pumped dye laser system (Quanta-Ray DCR1A/PDL1) was the source of the photolysis radiation, and the probe radiation was obtained from an excimer laser-pumped dye laser system (Lambda-Physik EMG 101 MSC/FL 2001). Both photolysis and probe dye outputs were frequency doubled; KDP R6G and C crystals (Interactive Radiation, Inc.) were used to generate photolysis radiation at 307–333 nm for excitation of the $S_1 \leftarrow S_0$ absorption band of FNO, and a BBO crystal (CSK Ltd.) was used to double the frequency of the probe output. NO fragments

were detected by laser-induced fluorescence (LIF) via the $A\,{}^{2}\Sigma^{+}\leftarrow X\,{}^{2}\Pi$ transition at 219–227 nm. The fluorescence was detected with a solar blind PMT (Hamamatsu R166UH) through an interference filter (Corion, 300 nm, 85 nm bandwidth) combined with a reflecting mirror (Acton Research Corp., AR-coated, 98% at 308 nm, normal incidence) which transmits at wavelengths < 290 nm. The photolysis pulse energy was ~3 mJ, while the probe pulse energy was maintained at < 40 μJ (5 mm diam.), in order to avoid saturation and dissociation of FNO by the 226 nm radiation. The FNO absorption cross section at 226 nm is comparable to the absorption cross section in the region of this work,[26] and the two photon dissociation/detection process is eliminated when $I_{\text{pr}} \ll I_{\text{ph}}$.

The two laser beams were collinear and counterpropagating, but perpendicular both to the PMT and to the pulsed valve. Both photolysis and probe lasers were maintained at a vertical polarization in the laboratory frame. Brewster angle windows appropriately oriented were placed at both photolysis and probe chamber ports to minimize reflections at window surfaces. The timing sequence was controlled by a homemade digital delay generator with 20 ns increments, and the delay between the pump and probe lasers was set at 80 ns. The observed LIF signals were normalized to both laser intensities. The signals from 20–30 laser firings were averaged for each data point.

FNO was synthesized according to the procedure of Wilson and Wilson.[27] Briefly, the synthesis involved slowly passing F_2 gas in 10% excess of its stoichiometric quantity over NO maintained at 77 K in a Teflon U tube. NO (MG Industries, 99.0% min. purity) was purified by trap-to-trap distillations using an isopentane slush bath (− 160 °C). F_2 (MG Industries, 98% min. purity) was used without further purification. The gas handling system was made of Teflon, stainless steel, and Monel, and passivated with ClF_3 to remove traces of water. FNO was purified by trap-to-trap distillations using n-propanol (− 127 °C) and isopentane slush baths to remove NO_2 and NO contaminations, respectively. The FNO sample was stored at 77 K in a Monel tube, and in the absence of traces of water, was stable for at least several weeks. Due to the existence of equilibrium between FNO and NO, it was impossible to completely eliminate NO contamination from the sample. However, since NO produced in the dissociation is rotationally hot ($j_{\text{min}} > 15.5$), while for the expansion-cooled NO contamination $j < 8.5$, the results reported here are essentially unaffected by NO contamination.

B. Absorption spectrum

The 300 K absorption spectrum shown in Fig. 1 was recorded on a Shimadzu UV-260 uv-visible recording spectrophotometer. It is similar to the absorption spectra reported by Johnston and Bertin,[28] Solgadi and Flament,[29] and Suter *et al.*[23] over the same spectral region. According to *ab initio* calculations of the electronic states of FNO,[23,29] the absorption in the region 265–333 nm is assigned to the $S_1 (1\,{}^{1}A'') \leftarrow S_0 (1\,{}^{1}A')$ electronic transition. The dynamical study of Suter *et al.*[23] shows that the long progression with about 1000 cm^{-1} intervals must be assigned to the NO

stretching coordinate (ν_1), which is in agreement with other XNO systems such as $CH_3ONO(S_1)$,[30] $HONO(S_1)$,[31] or $ClNO(T_1,S_1)$.[6,12,13,20–22] Adjacent to each ($\nu_1 00$) peak there is a smaller peak assigned to ($\nu_1 01$) upper levels, where one quantum of a predominantly bending mode (ν_3) is excited. The assignments are marked in Fig. 1.

The absorption spectrum of FNO between 350 and 250 nm has been interpreted in Ref. 23 in terms of the S_1-state PES (for fixed F–NO Jacobi-angle γ) and the time-dependent wave packet evolving on this surface. Briefly, the PES has a shallow potential pocket at small F–NO distances with a very low potential barrier (390 cm^{-1}) in the direction of the F + NO exit channel (see Sec. III). Since the barrier is located near the Franck–Condon (FC) point, the wave packet splits after a few femtoseconds into a directly dissociating part, which gives rise to the broad background in the calculated spectrum, and a smaller portion, which is trapped for some time in the inner region. With each successive oscillation of the latter in the shallow well a certain fraction leaks out into the fragment channel until the entire wave packet has completely left the interaction region. The periodic motion of the trapped part of the wave packet leads to the structured component of the absorption spectrum.

According to the two-dimensional calculation with fixed FNO angle, the second progression is due to excitation of the F–NO stretching mode. However, in their ground electronic states, the X–NO stretching and bending motions of FNO (Ref. 32), and likewise of ClNO (Ref. 33), are strongly mixed and ν_2 as well as ν_3 have contributions from both motions. It will become apparent below (see Secs. III and IV) that the same holds also for the vibrational motion in the S_1 state of FNO. The mode leading to the second progression in the spectrum thus combines bending motion as well as motion associated with the F–NO dissociation coordinate. Although the normal mode notation is probably not justified for a fast dissociating system like FNO(S_1), we nevertheless use it as a convenient notation for identifying peaks in the spectrum.

C. Rotational state distributions

Figure 2 shows rotational distributions of NO($v = v_1$) obtained following excitation of the ($00v_3$), ($10v_3$), and ($20v_3$) levels with $v_3 = 0$ and 1, respectively. In each case, the excitation wavelength corresponds to a peak in the absorption spectrum. Even though the production of NO in other vibrational levels is energetically possible, we find that when exciting v_1 quanta in the parent, NO in $v = v_1$ is predominantly formed. The rotational distributions in this "adiabatic channel" are the subject of the present paper, and distributions in NO($v < v_1$) will be reported in a forthcoming publication.[34] Rotational distributions for NO($^{2}\Pi_{1/2}$) and NO($^{2}\Pi_{3/2}$) were derived separately from the Q-branch lines which dominated the LIF spectra.[34] The rotational level populations were obtained by dividing each line intensity by its appropriate line strength, i.e., Hönl–London factor. The results are uncorrected for alignment effects.[35] FNO(S_1) dissociation yields comparable amounts of NO($^{2}\Pi_{3/2}$) and NO($^{2}\Pi_{1/2}$), but since the calculations re-
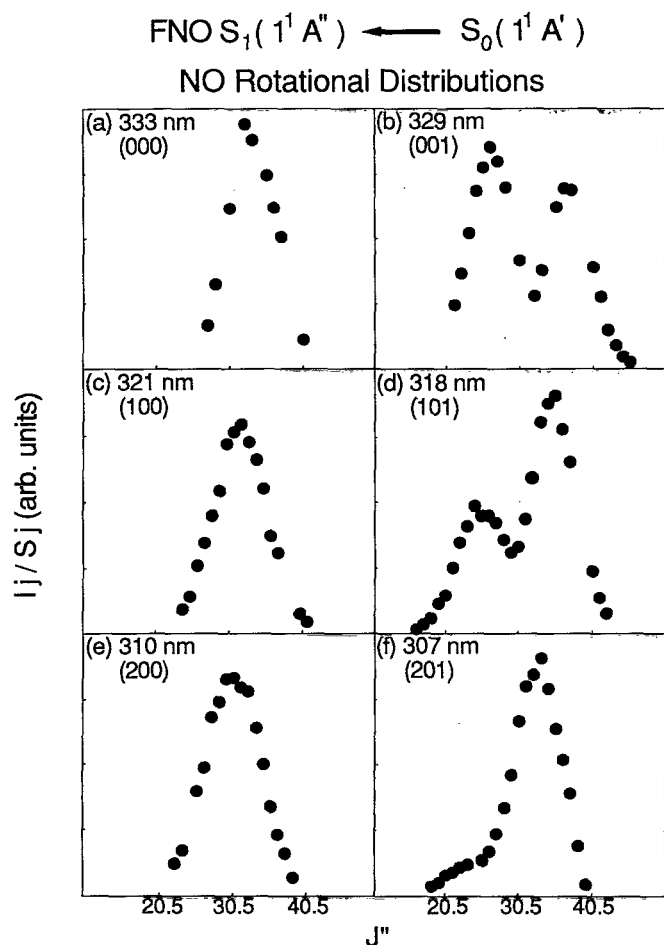
FIG. 2. Measured rotational state distributions of NO following excitation in the first six absorption peaks of the spectrum as indicated. The distributions on the left-hand side originate from the decay of states with $v_3 = 0$, while those on the right-hand side derive from states with $v_3 = 1$. NO in $v = 0$, 1, and 2 is monitored following excitation in the $(00v_3)$, $(10v_3)$, and $(20v_3)$ bands, respectively.

ported here do not distinguish between the spin–orbit states of NO, we plot the sum of the $NO(^2\Pi_{1/2})$ and $NO(^2\Pi_{3/2})$ contributions to each rotational level. Since a full analysis of the alignment effects has not been performed, only level populations are reported here. However, previous work on similar systems [e.g., $ClNO(S_1,T_1)$][6,12,20] has shown that the corrections do not affect strongly the shapes of the distributions.

Clearly, the rotational distributions are highly inverted, with the maximum in the distributions following excitation of $(v_1 00)$ levels around $j = 30$. Another distinct feature is the shift of the entire distribution to slightly lower quantum numbers with increasing excitation energy. A decrease in the peak of the distribution of two quantum numbers is obtained per quantum of NO stretch excited in FNO. The most striking feature in the distributions is, however, the bimodal structures observed when one quantum of bending vibration is excited in the S_1 state. Both intensity maxima in the distributions show similar spin–orbit and Λ-doublet population

ratios and, upon changing the polarization of the photolysis laser from vertical to horizontal, exhibit alignment typical of a perpendicular transition.[34] Also, the populations derived from the weaker P and R branches show the same bimodal behavior. Thus the bimodal structures arise from excitation to the S_1 state. Notice that the shapes of the distributions are sensitive to the number of v_1 quanta, with the lobe at lower rotational levels decreasing relative to the lobe at higher rotational levels as v_1 increases. As shown in the next section, the three-dimensional calculations reproduce the main structures of the measured distributions. Furthermore, in Sec. IV we demonstrate how they can be interpreted as reflections of the transition-state wave functions.

III. THEORY

A. Potential energy surface

The MCSCF *ab initio* calculations of this study were performed in the same manner as those described in Ref. 23. In order to consider the rotation of the NO moiety it is necessary to vary also the FNO bending angle in addition to the two stretching coordinates. The construction of the three-dimensional S_1 PES has been performed in scattering or Jacobi coordinates, R, r, and γ, which are subsequently employed in the dynamical calculations. R is the distance between the F atom and the center of mass of NO, r is the NO bond length, and the orientation angle γ is the angle between F, the center of mass of NO, and O. Complete two-dimensional surfaces in R and r have been determined for eight angles, $\gamma = 70°$, $90°$, $100°$, $110°$, $120°$, $128.37°$, $135°$, and $150°$. Energy values between the grid points were obtained by a three-dimensional spline procedure.

Figure 3 depicts contour plots in the (R,r) plane for five angles. $128.4°$ is the equilibrium orientation angle in the electronic ground state (corresponding to a FNO bond angle of $109.8°$, see Table I in Ref. 23) where the dissociation motion in the upper state begins, leading ultimately to dissociation. The very shallow potential barrier for $128.4°$, that has been found to be of utmost importance for the temporary trapping of some portion of the wave packet and the subsequent fragmentation into F and NO,[23] diminishes as the angle changes, especially with decreasing γ. The potential for $110°$ (not shown in the figure) is already purely repulsive, like the one for $100°$. A correct description of the γ dependence of the potential in the transition-state region is essential for the lifetime of the transient complex and hence for a good reproduction of the absorption spectrum. The MCSCF calculations considerably underestimate the dissociation energy requiring a modification of the original PES as described in Ref. 23. This modification affects only the potential in the exit channel and not in the inner region or the region of the transition state.

In the present article we focus the discussion on the rotational excitation of NO, and it is therefore appropriate to consider a 2D cut of the 3D PES featuring R and γ (Fig. 4). At each point in the (R,γ) plane the potential is minimized in the r direction. Such potential representations are helpful for the discussion of rotational excitation of the diatomic photofragment in the course of the dissociation.[13,36,37]
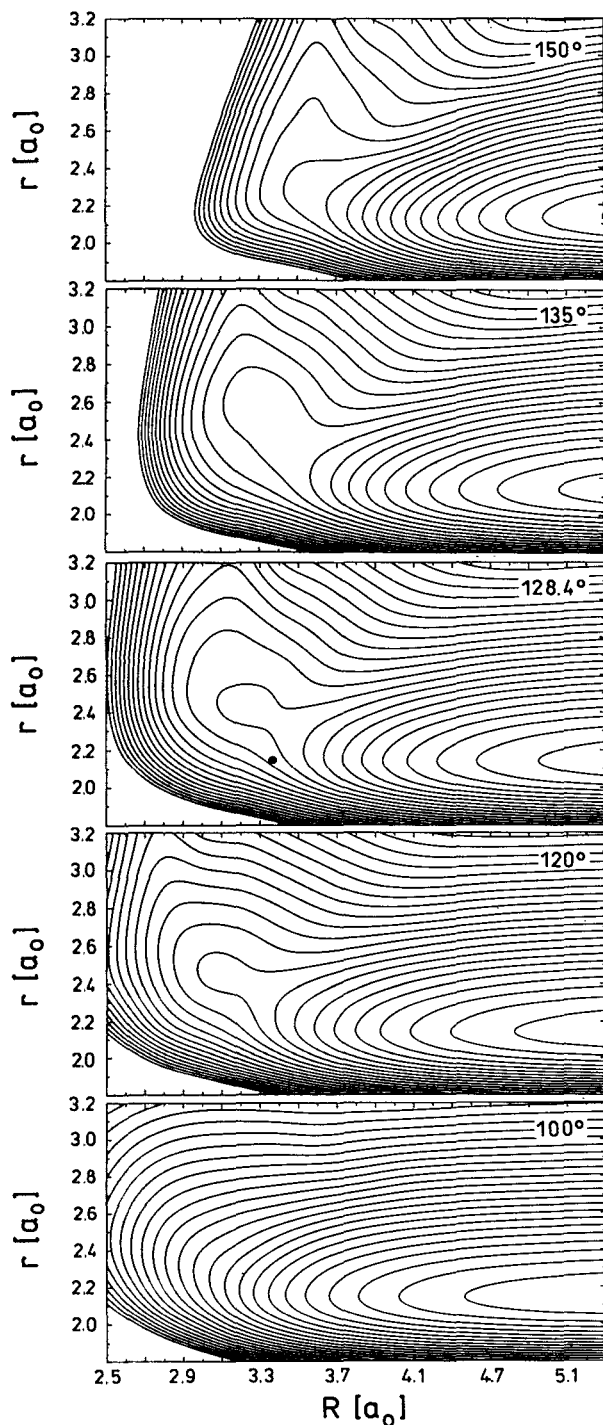
Downloaded 14 Jul 2010 to 128.125.205.65. Redistribution subject to AIP license or copyright; see http://jcp.aip.org/jcp/copyright.jsp

FIG. 4. Two-dimensional representation of the potential energy surface of $FNO(S_1)$. The potential is minimized along r, the NO stretching coordinate, for each set (R,γ). The energy spacing of the contours is 0.25 eV and the highest contour corresponds to 6 eV. The dot marks the equilibrium geometry of the ground electronic state and the arrow illustrates qualitatively the reaction path in the exit channel. The straight line represents the so-called transition line.

FIG. 3. Contour plots of the S_1 potential energy surface of FNO as a function of the Jacobi-coordinates R and r for fixed angles γ. R is the distance from the recoiling F atom to the center of mass of NO, r is the NO stretching coordinate, and γ is the Jacobi orientation angle. The dot in the plot for 128.4° marks the equilibrium geometry in the ground electronic state. The energy spacing is 0.25 eV and the highest energy is 6 eV. Energy normalization is such that $F + NO(r_e)$ corresponds to $E = 0$.

In accordance with Fig. 3, the potential in Fig. 4 has also a shallow pocket near the ground state equilibrium which is marked by the heavy dot. Because of a substantial inclination of the excited state 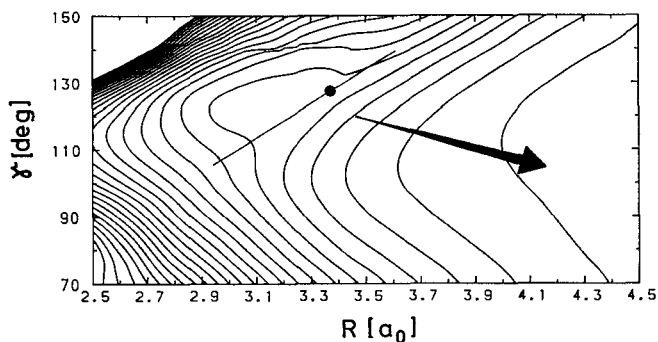potential well, the internal motion within this well is a mixture of bending and F–NO stretching motion associated with the coordinates γ and R as mentioned above (see also Sec. IV for plots of stationary wave functions). In order to simplify the subsequent discussion we will identify the motion that finally evolves into fragment rotation with a bending vibration. The vibration in the NO stretching coordinate is only weakly coupled to this mode.

Beyond the transition seam, indicated in a qualitative way by the straight line in Fig. 4, the potential is strongly repulsive and once the molecule has passed this region the two fragments rapidly separate. The dissociation path (represented by the arrow in Fig. 4) is also substantially tilted with respect to the R axis, which implies a relatively strong torque and therefore a strong rotational excitation of NO as actually observed in the experiment (see Fig. 2).

B. Three-dimensional wave packet dynamics

The dynamical calculations were performed in the time-dependent picture pioneered by Heller.[38] (See Chap. 4 of Ref. 3 for a comprehensive discussion.) We solve the time-dependent Schrödinger equation for a wave packet $\Phi(R,r,\gamma;t)$ with the initial condition that the wave packet at $t = 0$ equals the wave function for the lowest vibrational state of $FNO(S_0)$, i.e., the coordinate dependence of the transition dipole function (which has not been calculated) is ignored. The actual numerical solution of the Schrödinger equation including all three degrees of freedom proceeds in the same way as described in Ref. 39 for the dissociation of $ClNO(S_1)$.

In short, the wave packet is expanded in terms of the rotational eigenfunctions of the free NO fragment, $Y_{j0}(\gamma,\phi = 0)$, which leads to a set of N coupled partial differential equations for the expansion functions $\chi_j(R,r;t)$ with $j = 0,1,...,j_{max}$. A reduction in computer time is achieved if one additionally applies the *discrete variable representation* of Bačić and Light[40] which had not been utilized in Ref. 39. The propagation of the coupled two-dimensional wave packets $\chi_j(R,r;t)$ in space and time employs the fast-Fourier-transformation technique[41] and the Chebychev expansion
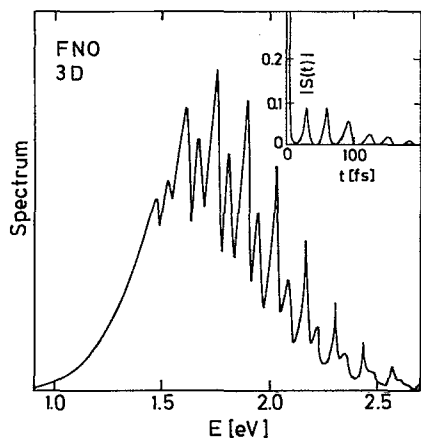
FIG. 5. Theoretical absorption spectrum $\sigma(E)$ calculated with the three-dimensional potential energy surface. Energy normalization is such that $E = 0$ corresponds to $F + NO(r_e)$. Note that in contrast to Fig. 1 the photolysis wavelength decreases from left to right. As in the experimental spectrum the main progression corresponds to excitation of the NO stretching motion with quantum numbers $v_1 = 0,1, \cdots$ and the second, less intense progression is assigned to bending excitation with $v_3 = 1$. The inset shows the modulus of the autocorrelation function $S(t)$ as defined in the text. The period of the recurrences, T_{NO} is related to the energy spacing of the main progression by $\Delta E = 2\pi/T_{NO}$.

method of Tal-Ezer and Kosloff.[42] Reference 39 contains a detailed description of how the final state distributions of NO are extracted from the wave packet in the limit $t \to \infty$.

Since the degree of rotational excitation of NO is large, $N = 60$ rotational expansion functions are required for convergence. A 96×56 grid in the (R,r) plane is used in the Fourier expansion technique. The propagation in time can be stopped after about 300 fs, because at this point the entire wave packet moves freely in the asymptotic region where the translational and the internal degrees of freedom are no longer coupled.

The initial wave packet $\Phi(R,r,\gamma;0)$ is taken as the product of three Gaussian functions in R, r, and γ with equilibrium positions $R_e = 3.376\,a_0$, $r_e = 2.142\,a_0$, and $\gamma_e = 128.37°$ as obtained from the MCSCF calculations in Ref. 23. The exponents, derived from the experimental frequencies,[43] are $\alpha_R = 37.00\,a_0^{-2}$, $\alpha_r = 58.21\,a_0^{-2}$, and $\alpha_\gamma = 58.91\,\text{rad}^{-2}$. They correspond to full widths at half-maximum of $\Delta R = 0.274\,a_0$, $\Delta r = 0.221\,a_0$, and $\Delta\gamma = 12.43°$, respectively.

C. Absorption spectrum

The FC region is very close to the small barrier in the potential (see Figs. 3 and 4), i.e., the excitation pulse prepares the molecule in a configuration close to the transition state. After the wave packet $\Phi(R,r,\gamma;t)$ is launched in the S_1 state, it will quickly split into two parts, the major portion directly dissociates yielding F and rotationally excited NO and the remaining part is trapped inside the potential pocket for several vibrational periods. After each period a further splitting occurs. The modulus of the autocorrelation function $S(t) = \langle \Phi(0)|\Phi(t)\rangle$, shown in the inset of Fig. 5, mir-

rors the motion of the wave packet in the inner region of the S_1 PES. The sequence of recurrences with period $T_{NO} \approx 30$ fs represents the oscillation of the wave packet along the NO stretching coordinate. The autocorrelation function is the link between the time-dependent dynamics on the one hand, and the energy-dependence of the spectrum $\sigma(E)$ on the other hand.[38] $S(t)$ and $\sigma(E)$ are related to each other by a Fourier transformation.

Figure 5 shows the calculated absorption spectrum $\sigma(E)$ as a function of the energy in the excited state. [Normalization is such that $F + NO(r_e)$ corresponds to $E = 0$.] It consists, like the experimental spectrum and the spectrum obtained in Ref. 23 for a fixed angle γ, of a broad background superimposed by two progressions. The broad background in the calculated $S_1 \leftarrow S_0$ absorption spectrum is due to the direct part of the wave packet, and the relatively sharp structures (resonances) superimposed on the background are the consequence of the trapped portion of $\Phi(t)$. The main progression is associated with the NO stretch, whereas the second progression is due to excitation of a mode which combines bending and stretching along the dissociation coordinate R. The corresponding frequencies $\omega_1 = 1120$ cm^{-1} and $\omega_3 = 450$ cm^{-1} agree satisfactorily with the experimental values of 1045 and 340 cm^{-1}.[23] In comparison to the 2D calculation in Ref. 23, the NO frequency is increased by roughly 8%.

In contrast to the 2D or the experimental spectrum, the background is overemphasized and, in addition, the widths of the superimposed structures are too large. In terms of the time-dependent picture, the trapped portion of the wave packet is too small and, moreover, its survival time in the potential pocket is too short. In comparison to the 2D calculation of Ref. 23, the first recurrence of the 3D autocorrelation function is roughly a factor of 2 smaller and the sequence of maxima diminishes twice as fast. This points to subtle inaccuracies in the calculated 3D potential in the transition-state region, particularly the angle dependence of the very small potential barrier. As $FNO(S_1)$ starts to dissociate, the bending angle first decreases due to the strong repulsion between F and N. Since the barrier height decreases with γ, the motion in γ promotes the leakage of the trapped portion of the wave packet and, consequently, the survival time in the complex region significantly diminishes with respect to the 2D calculation for which the angle is frozen.

The inaccuracies in the present calculations concerning subtle features of the PES topology in the transition-state region are very small, and it will be extremely difficult to improve the calculated energies any further. Nevertheless, for the purpose of the present study our MCSCF potential is sufficiently accurate to clearly demonstrate the dependence of the rotational state distributions of the NO fragment on the degree of bending excitation of the parent molecule before the final bond rupture.

D. Rotational state distributions

Figure 6 depicts the calculated rotational state distributions that correspond to the measured distributions in Fig. 2. The final vibrational quantum number of NO is identical to the quantum number v_1 in $FNO(S_1)$. In accord with the
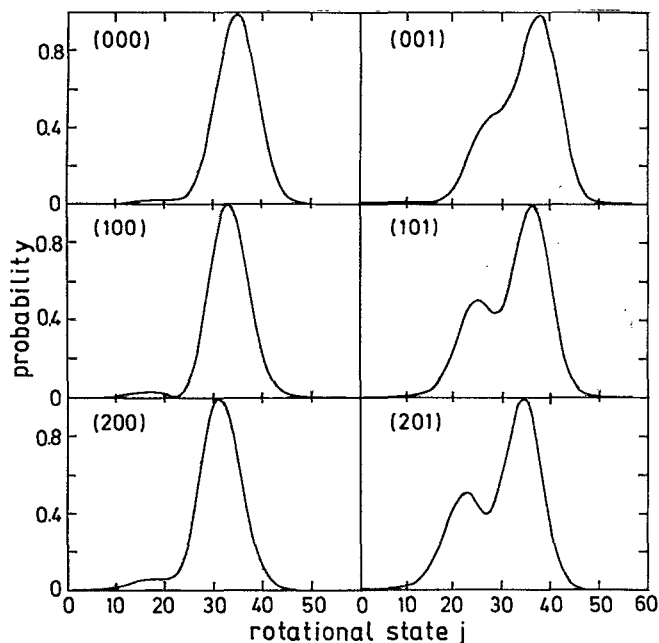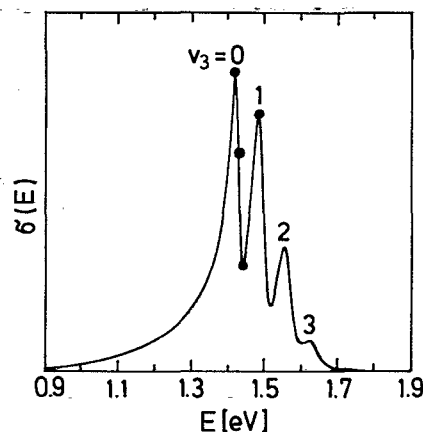
FIG. 7. Theoretical absorption spectrum as obtained in the two-dimensional model in which the NO stretching degree of freedom is frozen. According to the normal mode assignment the peaks are labeled as $(00v_3)$ with the bending quantum number $v_3 = 0$, 1, 2, and 3. The dots mark the energies used in Fig. 10, which demonstrates the sensitivity of the rotational distributions to the exact energy position relative to the resonance peaks.

FIG. 6. Calculated rotational state distributions of NO following excitation in the $(v_1 00)$ peaks (left-hand panels) and the $(v_1 01)$ peaks (right-hand panels). The vibrational quantum number of NO is always $v = v_1$, as in Fig. 2. The top, middle, and bottom panels correspond to excitation in $v_1 = 0$, 1, and 2, respectively. These calculations involve all three degrees of freedom of FNO.

measurement, the excitation of $FNO(S_1)$ in vibrational states with $v_3 = 0$ leads to Gaussian-type distributions with maxima between 30 and 35. The widths are $\Delta j \approx 10$ in good agreement with $\Delta j \approx 9$ for the experimental distributions. In full agreement with the experiment, the maximum shifts to lower states by about two quanta with each quantum of the NO stretch, v_1. This shift is a consequence of the fact that the NO stretching frequency within the S_1 state is significantly smaller than for the free NO molecule. Therefore, an increasingly smaller portion of the total available energy can be partitioned into translation and rotation with increasing NO stretching quantum numbers $v_1 = v$.

As in the experiment, the distributions following the decay of the excited bending states with $v_3 = 1$ have a bimodal shape with the relative heights of the two peaks depending on the NO stretching quantum number v_1. However, the calculated distributions show a trend with v_1 opposite to the observed one. Besides this discrepancy, the theoretical distributions agree well with the measured distributions as far as the locations of the maxima, the overall width, and the shift with the NO stretching quantum number are concerned. Possible explanations for the different trends of the intensity ratio in experiment and theory will be discussed in Sec. V.

The bimodal shapes of the distributions for $v_3 = 1$ reflect the nodal behavior of the corresponding wave functions along the "transition line" which separates the very shallow potential well from the strongly repulsive exit channel. In order to illustrate convincingly the reflection principle, we

present in the next section two-dimensional calculations using the potential shown in Fig. 4. The analysis follows essentially the treatments of Refs. 15 and 16. Freezing the NO stretching degree of freedom has—besides some purely technical benefits—the advantage that the decay of higher bending states ($v_3 = 2$ and 3) can be investigated without overlap with states of higher v_1. These states give rise to even more structured final rotational state distributions.

IV. MAPPING OF TRANSITION-STATE WAVE FUNCTIONS

Figure 7 shows the absorption spectrum calculated with the two-dimensional PES displayed in Fig. 4; the NO stretching degree of freedom is not taken into account in the following analysis. This spectrum corresponds to excitation of merely one NO-stretch vibrational quantum, and therefore is simpler and considerably narrower than the observed spectrum. As briefly discussed in Sec. III, it consists of a background superimposed by a progression of narrower bands. The latter are assigned to excitation of a combination of bending and F–NO stretching vibration as the stationary wave functions in Fig. 8 clearly manifest. These wave functions solve the time-independent Schrödinger equation for fixed energies E corresponding to the four resonance maxima in the absorption spectrum shown in Fig. 7. They can be calculated either in the time-independent approach of photodissociation (see Ref. 3, Chap. 2) or by Fourier transformation of the evolving wave packet,

$$\Psi(R,\gamma;E) \propto \int dt\, \Phi(R,\gamma;t)e^{iEt}. \qquad (1)$$

The stationary wave functions contain the entire history of the dissociation process and therefore illustrate the reaction path and the portion of the PES sampled during the breakup. Inside the shallow potential well they behave like bound-state wave functions with an apparent nodal structure, while
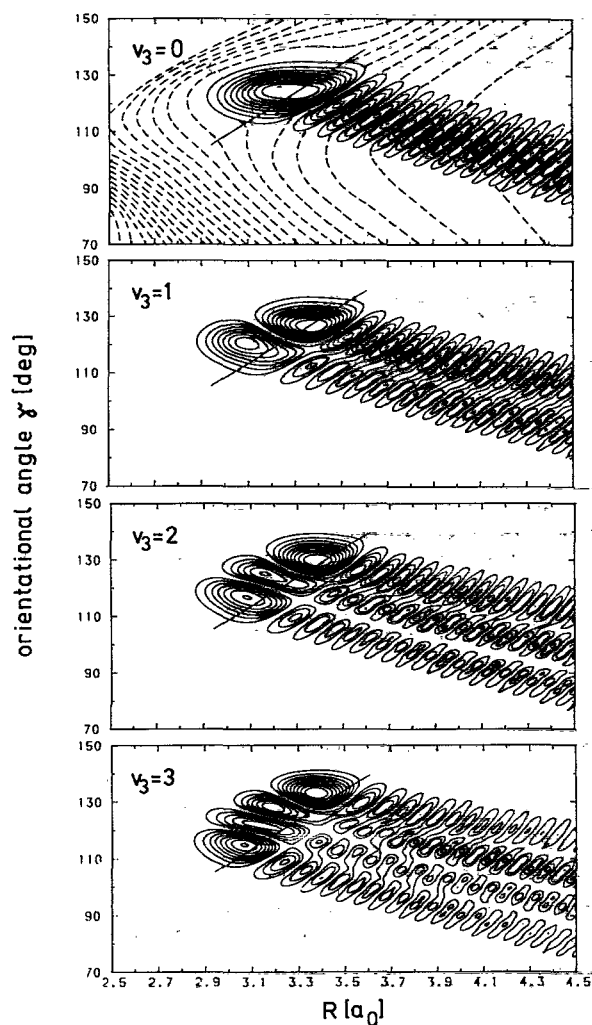
FIG. 8. Contour plots of the stationary wave functions $\Psi(R,\gamma;E)$ defined in Eq. (1) for the four lowest bending resonances in Fig. 7 corresponding to $v_3 = 0$, 1, 2, and 3. The straight lines indicate the transition line.

tum mechanical distribution function on the transition line, i.e., the modulus square of the transition-state wave function $|\Psi_{ts}(\gamma_0;E)|^2$.

The classical distribution is now defined by

$$P_{cl}(j) \propto \sum \sin \bar{\gamma}_0 |\Psi_{ts}(\bar{\gamma}_0)|^2 \left| \frac{dJ}{d\gamma_0} \right|^{-1}_{\gamma_0 = \bar{\gamma}_0(j)}, \qquad (2)$$

where the relation between the rotational angular momentum quantum number j on one hand and the orientation angle $\bar{\gamma}_0(j)$ on the other hand is given by

$$J(\bar{\gamma}_0) = j. \qquad (3)$$

The sum in Eq. (2) extends over all trajectories specified by initial angles $\bar{\gamma}_0(j)$ which lead to the designated final rotational angular momentum. If the relation between j and γ_0 is unique, i.e., for each final rotational state there exists exactly one trajectory, the sum collapses to a single term. Under such circumstances the final rotational state distribution is essentially a reflection of the weighting function $|\Psi_{ts}(\gamma_0)|^2$ onto the quantum number axis mediated by the excitation function $J(\gamma_0)$.

The left-hand side of Fig. 9 depicts the rotational excitation function together with the weighting function $|\Psi_{ts}(\gamma_0)|^2$ corresponding to the energies of the four bending resonances. Since the curvature of $J(\gamma)$ is small the extra factor $|dJ/d\gamma_0|^{-1}$ can be ignored for the present qualitative discussion. The corresponding *quantum mechanical* rotational state distributions obtained in the 2D model are depicted on the right-hand side of Fig. 9. The reflection principle is clearly evident and needs no further explanation. Each maximum or minimum in the distribution has a counterpart in the weighting function. The reflection principle works well even for relatively large bending excitation when the corresponding wave function oscillates appreciably. Merely the intensity ratios, especially those for the smaller reflection maxima, are less satisfactorily explained by the simple classical picture. However, one should bear in mind, that the transition line, and thus the transition-state wave function, is not rigorously defined. Slight variations of the transition line can certainly influence the more subtle details.

The reflection structures in the final rotational state distributions are analogous to the reflection structures observed in the emission spectra of diatomic molecules for the transition from a bound upper state to a repulsive lower state.[44] In the present case, however, the reflection is mediated by the excitation function which is dynamically defined (by running classical trajectories), whereas in the case of emission spectra the potential itself mediates the reflection of the quantum mechanical distribution function.

Finally, it is interesting to follow the development of the reflection structures as a function of energy from one resonance to the next. Figure 10 depicts calculated state distributions for four values of increasing energy from the $v_3 = 0$ to the $v_3 = 1$ resonance. The variation across the resonance is continuous but not straightforward; the shape of the distribution depends sensitively on whether one excites directly in the peak of a resonance, in the wings, or in between two adjacent resonances.

beyond the transition-state region they have the appearance of continuum wave functions. Owing to the large reduced mass and the relatively high translational energy, the de Broglie wavelength is quite small in the exit channel.

Following our earlier work,[15,16] we consider the final step of the bond fission to start on the transition line, that is indicated by the straight line in Figs. 4 and 8. Once the molecule has passed this limit, the F–NO bond breaks. Furthermore, it is assumed that the rotational excitation of NO takes place exclusively in the exit channel, while the motion in the intermediate well is important only for the determination of the "initial conditions" on the transition line for the subsequent bond rupture.

According to the classical methodology established for direct photodissociation,[7–10] we start classical trajectories on the transition line and follow their course downhill towards the product channel. The final rotational angular momentum $j(t \to \infty)$ is a function of the initial orientation angle γ_0 which we call the *rotational excitation function* $J(\gamma_0)$. Each individual trajectory is weighted by the quan-
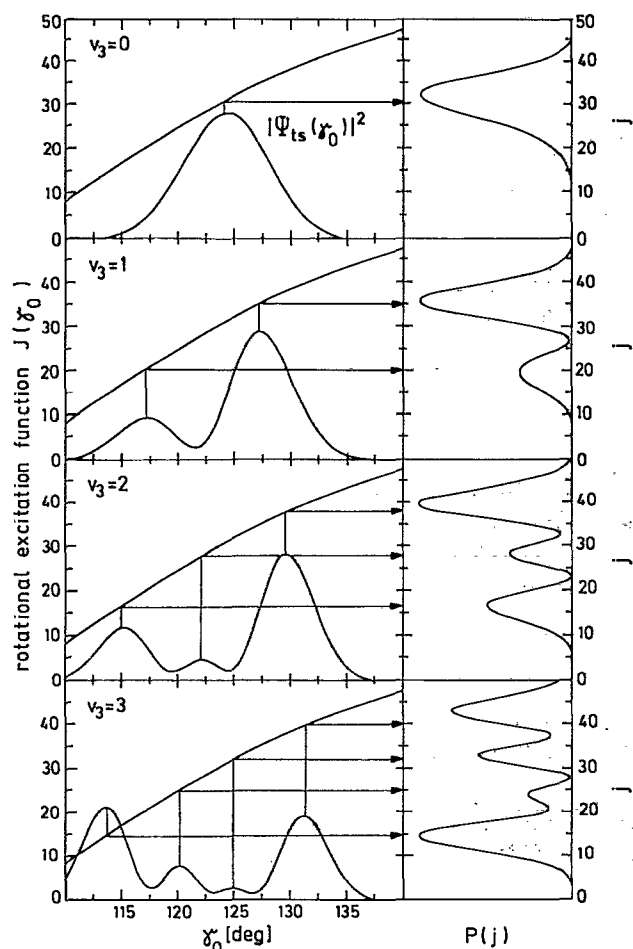
FIG. 9. Left-hand side: Rotational excitation function $J(\gamma_0)$ as defined in the text. Also shown are the transition-state wave functions $|\Psi_{ts}(\gamma_0)|^2$, i.e., cuts along the transition line through the two-dimensional wave functions depicted in Fig. 8. Right-hand side: The corresponding *quantum mechanical* rotational state distributions obtained in the two-dimensional model. The arrows illustrate the reflection principle.

V. SUMMARY AND CONCLUSIONS

In this study we present the first example for which fragment rotational distributions map the parent transition-state wave functions in the presence of strong final-state interaction. It is shown that in the photodissociation of $FNO(S_1)$, excitation in $v_3 = 0$ bending vibronic states results in NO fragments with Gaussian-type rotational state distributions with maxima at high rotational levels ($j \approx 30.5$; $\Delta j = 10$), while excitation involving $v_3 = 1$ bending states yields bimodal distributions. The bimodality persists even when $v_3 = 1$ excitation is mixed with excitation of the NO stretching degree of freedom in the parent molecule ($v_1 = 1$ and 2). However, the exact shape of the distributions, i.e., the ratio of the two maxima, depends sensitively on the number of v_1 quanta.

The rotational distributions are well reproduced by time-dependent wave packet calculations performed on a three-dimensional PES determined by *ab initio* methods. The extent of rotational excitation and the overall width of
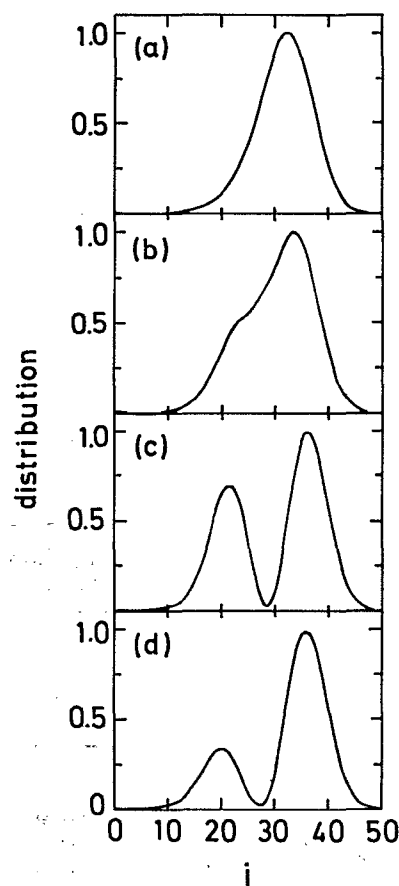

FIG. 10. Rotational state distributions for the four energies indicated by the dots in the spectrum shown in Figs. 7. (a) and (d) correspond to the $v_3 = 0$ and the $v_3 = 1$ resonances, respectively.

the distributions are predicted very well. Most importantly, the *ab initio* calculation reproduces the distinct dependence on the bending state excited in the parent molecule: $v_3 = 0$ levels lead to Gaussian-type rotational state distributions while fragmentation of $v_3 = 1$ states yields bimodal distributions. Only the exact ratios of the two maxima and their dependence on the NO stretching quantum number v_1 show discrepancies with the experimental results.

The salient features of the rotational distributions, i.e., the bimodalities following $v_3 = 1$ excitation, are also well reproduced by two-dimensional calculations for which the NO bond distance has been frozen. These calculations also enable us to predict the rotational distributions obtained with $v_3 = 2$ and 3 excitation, which are not observed experimentally due to spectral overlap. We find that the corresponding rotational state distributions have three and four maxima, respectively.

Using classical trajectories in combination with the rotational reflection principle, we demonstrate that the rotational state distributions reflect in a unique way the nodal structures of the associated (stationary) wave functions at the transition state. The shape of the wave function in the direction roughly perpendicular to the dissociation path is mapped onto the rotational quantum number axis. This

mapping is mediated by the rotational excitation function and hence by the final-state interaction (i.e., the torque) in the exit channel when the two fragments recoil. The nodal structure of the wave function is preserved even in the presence of significant translational–rotational coupling.

The present results demonstrate that the shapes of the rotational distributions with their associated nodes depend on two factors: First, the shape of the bending wave function at the transition state; and second, the strength of the final-state interaction that determines the evolution of the wave function in the exit channel, beyond the barrier. Furthermore, the shape of the transition-state wave function depends on the depth and the shape of the potential well near the FC region and the form of the PES around the transition state. The mode couplings between vibrational and translational degrees of freedom may cause broadening of the dissociation wave functions and hence loss of the modal structures. In summary, the final rotational state distributions and especially their possible modal structures are sensitive probes of the multidimensional potential energy surface.

The high sensitivity of the distributions to subtle features of the PES may be one possible reason for the discrepancy between experiment and theory concerning the intensity ratios of the two maxima following $v_3 = 1$ excitation. The resonance structures in the 3D spectrum (Fig. 5) are noticeably too broad as compared to the experimental spectrum and moreover, the background is overestimated at the expense of the vibrational structures. This is particularly apparent for the $v_1 = 0$ band. Adjacent resonances overlap considerably and this overlap, which is much smaller in the experimental spectrum or the 2D calculation, might also affect the rotational state distributions. In addition, the underlying continuum, which is responsible for the direct dissociation channel, may also contribute. In Fig. 10 we have illustrated that the exact shape of the rotational distribution depends sensitively on whether the excitation is directly on a resonance peak or in the wings; the same holds for the 3D calculation. The fact that the (001) resonance yields merely a shoulder in the distribution rather than a clearly resolved second peak might be the result of the substantial overlap with the (000) and the (001) resonances. For example, calculating the rotational state distribution at a slightly higher energy than the (001) resonance energy changes the shoulder into a clear second maximum. Due to the coexistence of direct and indirect fragmentation, i.e., the "interference" of the background with the resonances, the dissociation of FNO is a very complex process demanding an extraordinarily high precision of the PES.

In addition, experimental uncertainties may add to the discrepancy as well. A complete data analysis taking into account alignment effects and the variation of the Λ-doublet ratios with rotational quantum number may also modify the ratio of the two maxima in the distributions.

Reflection-type structures in rotational state distributions are probably common features in many photodissociation processes provided the absorption spectrum exhibits bands due to excitation of bending states within the transient complex. They manifest in a distinct way the dependence of photodissociation cross sections on the initial quantum state

prepared in the parent molecule. The dissociation of FNO is a fine example of quantum state selectivity in molecular dynamics.

[1] M. N. R. Ashfold and J. E. Baggott, *Molecular Photodissociation Dynamics* (Royal Society of Chemistry, London, 1987).

[2] H. Reisler and C. Wittig, in *Chemical Kinetics and Dynamics*, edited by J. A. Barker (JAI, Greenwich, 1992); C. X. W. Qian and H. Reisler, in *Advances in Molecular Vibrations and Collision Dynamics*, edited by J. M Bowman (JAI, Greenwich, 1991).

[3] R. Schinke, *Photodissociation Dynamics* (Cambridge University, Cambridge, 1992).

[4] P. Andresen, V. Beushausen, D. Häusler, H. W. Lülf, and E. Rothe, J. Chem. Phys. 83, 1429 (1985); D. Häusler, P. Andresen, and R. Schinke, *ibid.* 87, 3949 (1987).

[5] R. L. Vander Wal and F. F. Crim, J. Phys. Chem. 93, 5331 (1989); R. L. Vander Wal, J. L. Scott, and F. F. Crim, J. Chem. Phys. 94, 1859 (1991); R. L. Vander Wal, J. L. Scott, F. F. Crim, K. Weide, and R. Schinke, *ibid.* 94, 3548 (1991).

[6] C. X. W. Qian, A. Ogai, L. Iwata, and H. Reisler, J. Chem. Phys. 89, 6547 (1988); Y. Y. Bai, A. Ogai, C. X. W. Qian, L. Iwata, G. A. Segal, and H. Reisler, *ibid.* 90, 3903 (1989).

[7] R. Schinke, Ann. Rev. Phys. Chem. 39, 39 (1988).

[8] R. Schinke, Comments At. Mol. Phys. 23, 15 (1989).

[9] R. Schinke, J. Chem. Phys. 85, 5049 (1986).

[10] R. Schinke and V. Engel, Faraday Discuss. Chem. Soc. 82, 111 (1986).

[11] A. Ticktin, A. E. Bruno, U. Brühlmann, and J. R. Huber, Chem. Phys. 125, 403 (1988); A. E. Bruno, U. Brühlmann, and J. R. Huber, Chem. Phys. 120, 155 (1988).

[12] A. Ogai, C. X. W. Qian, L. Iwata, and H. Reisler, Chem. Phys. Lett. 146, 367 (1988).

[13] R. Schinke, M. Nonella, H. U. Suter, and J. R. Huber, J. Chem. Phys. 93, 1098 (1990).

[14] R. Schinke, R. L. Vander Wal, J. L. Scott, and F. F. Crim, J. Chem. Phys. 94, 283 (1991).

[15] R. Schinke, A. Untch, H. U. Suter, and J. R. Huber, J. Chem. Phys. 94, 7929 (1991).

[16] A. Vegiri, A. Untch, and R. Schinke, J. Chem. Phys. 92, 3688 (1992).

[17] U. Brühlmann and J. R. Huber, Chem. Phys. Lett. 143, 199 (1988).

[18] A. Untch, K. Weide, and R. Schinke, Chem. Phys. Lett. 180, 265 (1991).

[19] R. N. Dixon and H. Rieley, J. Chem. Phys. 91, 2308 (1989).

[20] C. X. W. Qian, A. Ogai, L. Iwata, and H. Reisler, J. Chem. Phys. 92, 4296 (1990).

[21] C. X. W. Qian, A. Ogai, J. Brandon, Y. Y. Bai, and H. Reisler, J. Phys. Chem. 95, 6763 (1991).

[22] D. Sölter, H.-J. Werner, M. von Dirke, A. Vegiri, A. Untch, and R. Schinke (to be published).

[23] H. U. Suter, J. R. Huber, M. von Dirke, A. Untch, and R. Schinke, J. Chem. Phys. (in press).

[24] A. Ogai, C. X. W. Qian, and H. Reisler, J. Chem. Phys. 93, 1107 (1990).

[25] D. Proch and T. Trickl, Rev. Sci. Instrum. **60**, 713 (1989).

[26] A. Ogai, J. Brandon, and H. Reisler (unpublished results).

[27] W. Wilson and R. Wilson (private communication).

[28] H. S. Johnston and H. J. Bertin, Jr., J. Mol. Spectrosc. **3**, 683 (1959).

[29] D. Solgadi and J. P. Flament, in *Photophysics and Photochemistry Above 6 eV*, edited by F. Lahmani (Elsevier, Amsterdam, 1985), p. 497.

[30] M. Nonella and J. R. Huber, Chem. Phys. Lett. **131**, 376 (1986); S. Hennig, V. Engel, R. Schinke, M. Nonella, and J. R. Huber, J. Chem. Phys. **87**, 3522 (1987).

[31] S. Hennig, A. Untch, R. Schinke, M. Nonella, and J. R. Huber, Chem. Phys. **129**, 93 (1989).

[32] L. H. Jones, L. B. Asprey, and R. R. Ryan, J. Chem. Phys. **47**, 3371 (1967); S. C. Foster and J. W. C. Johns, J. Mol. Spectrosc. **103**, 176 (1984).

[33] L. H. Jones, R. R. Ryan, and L. B. Asprey, J. Chem. Phys. **49**, 581 (1968).

[34] J. Brandon, A. Ogai, and H. Reisler (to be published).

[35] The dominance of the Q-branch results from Λ-doublet preferences, modified by alignment effects.

[36] R. Schinke, J. Chem. Phys. **92**, 2397 (1990).

[37] M. Nonella, J. R. Huber, A. Untch, and R. Schinke, J. Chem. Phys. **91**, 194 (1989).

[38] E. J. Heller, Acc. Chem. Res. **14**, 368 (1981); in *Potential Energy Surfaces and Dynamics Calculations*, edited by D. G. Truhlar (Plenum, New York, 1981).

[39] A. Untch, K. Weide, and R. Schinke, J. Chem. Phys. **95**, 6496 (1991).

[40] Z. Bačić and J. C. Light, J. Chem. Phys. **85**, 4594 (1986).

[41] R. B. Gerber, R. Kosloff, and M. Berman, Comput. Phys. Rep. **5**, 59 (1986); R. Kosloff, J. Phys. Chem. **92**, 2087 (1988).

[42] H. Tal-Ezer and R. Kosloff, J. Chem. Phys. **81**, 3967 (1984).

[43] C. Cazzoli, C. Degli Eposti, P. G. Favero, and P. Palmeri, Nuovo Cimento **3**, 627 (1984).

[44] J. Tellinghuisen, in *Photodissociation and Photoionization*, edited by K. P. Lawley (Wiley, New York, 1985).